Biosurface and Biotribology

WILEY

The Institution of Engineering and Technology

ORIGINAL RESEARCH OPEN ACCESS

A Mechanical Study of a Flexible Composite Coating at the Dental Implant–Bone Interface Using Finite Element Analysis

Hui Yan[1] | Mengkai Lu[1] | Wenkai Zheng[1] | Yuan Jin[1] | Guangyong Li[1] | Bin Huang[1] | Jianke Du[1] | Minghua Zhang[1] | Licheng Hua[1,2]

[1]Zhejiang-Italy Joint Lab for Smart Materials and Advanced Structures, School of Mechanics and Engineering Science, Ningbo University, Ningbo, Zhejiang, China | [2]Key Laboratory for Intelligent Nano Materials and Devices of Ministry of Education, Nanjing University of Aeronautics and Astronautics, Nanjing, Jiangsu, China

Correspondence: Licheng Hua (hualicheng@nbu.edu.cn)

Received: 11 December 2025 | **Revised:** 23 April 2026 | **Accepted:** 30 April 2026

Keywords: dental implant | finite element analysis | flexible composite coating | implant-alveolar bone interface

ABSTRACT

Damage to the dental implant–alveolar bone interface is one of the key issues limiting the service life of implants, whereas the periodontal ligament between natural teeth and the alveolar bone provides a flexible cushioning function for the interface. Inspired by the flexible cushioning function of the periodontal ligament, this study comparatively analyses the mechanical properties of the dental implant–alveolar bone interface before and after adding a periodontal ligament-like flexible composite coating to the implant surface through finite element computer simulations, aiming to investigate the interfacial cushioning effect of the flexible composite coating. The results demonstrate that the flexible composite coating reduces and redistributes the stress at the implant–alveolar bone interface, providing an interfacial cushioning effect. Furthermore, both the application method and thickness of the flexible composite coating influence the interfacial cushioning to a certain extent. This research holds theoretical significance for the development of next-generation dental implants and offers theoretical support for designing implants with flexible cushioning capabilities.

1 | Introduction

Dental implantation is currently one of the most commonly used clinical techniques for restoring tooth loss. It can replicate the aesthetic appearance of natural teeth and restore chewing function, earning it the title of 'the third set of human teeth' [1, 2]. Tooth loss is a widespread phenomenon globally. From ancient times to the modern era, people have continuously attempted to use various materials implanted into the jawbone to replace missing teeth, often resulting in widespread failure due to an inability to meet the complex demands of the oral environment. In 1969, Brånemark et al. [3] discovered that animal bone tissue could tightly integrate with titanium metal, leading to the successful biomimetic design of an 'osseointegrated artificial dental implant'. The principle involves implanting a medical-grade titanium fixture into the jawbone at the site of the missing tooth, where the implant surface fuses with the alveolar bone through osseointegration. A crown or bridge is then attached to the implant. This is currently one of the best methods for restoring tooth loss. However, clinical evidence shows that dental implants in many patients experience loosening and failure [4–7]. The causes of dental implant loosening are diverse and generally fall into two categories: biological complications [8, 9] and mechanical complications [10]. Biological complications include surgical-related issues such as bleeding, nerve injury and postoperative infections. Mechanical complications primarily involve issues with the prosthesis, such as fractures of screws, abutments or the implant itself. Mechanical complications can be further divided into two main categories [10, 11]. The first category is related to unscientific implant design. If the implant is not manufactured with precise dimensions tailored to the individual patient's anatomy, it can lead to uneven stress distribution, causing localised overload. This can result in micro-fractures of the surrounding bone, bone resorption, a series of inflammatory responses and ultimately, implant loosening and failure. For implant loosening caused by this type of issue, improving manufacturing precision and selecting appropriate thread designs based on the patient's specific conditions can generally reduce the incidence of loosening. The second category involves problems at the implant–bone tissue interface. Currently, the connection between clinical dental implants and bone primarily relies on a mechanical interlocking method similar to industrial bolts. However, unlike the micromotion at industrial fastener interfaces, the micromotion at the dental implant–bone interface represents minute relative movements between an artificial biomaterial and natural bioactive material in a specific biological environment. This not only affects damage at the implant–bone interface but also stimulates cellular pathways, leading to adverse biological effects such as bone resorption and fibrosis, which can ultimately cause interface failure and other related issues [4, 12, 13]. Micromotion damage at the dental implant–bone interface is one of the key issues limiting the service life of implants [4, 14, 15]. The micromotion damage at the interface is typically influenced by a combination of factors, including irrational implant design, uneven distribution of occlusal forces and various pathological conditions. Because of its movement amplitude being less than 100 μm, micromotion was often overlooked in previous dental implant research. It was not until 2004 that Zhou et al. [16] highlighted the impact of micromotion on the failure of dental implant systems, drawing researchers' attention to this phenomenon. Occlusal force is a critical mechanical factor directly affecting the stability and service life of dental implants. Individuals of different ages, genders and oral health conditions exhibit notable variations in masticatory loads [17, 18]. Furthermore, the distribution of masticatory loads varies with tooth position, with posterior teeth bearing the majority of the occlusal load, which is substantially higher than that of anterior teeth [19]. However, current clinical dental implants typically connect to the bone via a method similar to the mechanical interlocking of industrial bolts. This connection method inevitably leads to micromotion at the implant–bone interface, which has become a critical bottleneck restricting implant longevity. In reality, through long-term natural evolution, natural teeth can withstand a certain degree of physiological micromotion under normal conditions. A layer of periodontal ligament tissue forms a flexible cushioning connection between the tooth root and the alveolar bone, enabling the root-bone interface to endure millions of relative motion cycles while remaining intact. Therefore, inspired by the flexible cushioning function of the periodontal ligament, investigating the influence of designing a flexible structural layer on the implant surface that mimics the periodontal ligament's function on the mechanical properties of the implant–alveolar bone interface holds theoretical significance for the development of next-generation dental implants.

Since 2020, our team has begun exploring the design of flexible composite coatings on implant surfaces [20], and has conducted corresponding research on their micromechanical properties [21], biocompatibility [22] and tribological performance [23, 24]. Building upon this preliminary work, this paper investigates the influence of adding a flexible composite coating to the implant surface on the mechanical properties of the implant–alveolar bone interface through finite element simulations. It also compares the effects of different application methods and thicknesses of the flexible composite coating on the mechanical performance of the implant–alveolar bone interface, aiming to provide theoretical support for the development of implants with flexible cushioning capabilities.

2 | Experiments and Methods

2.1 | Model Source and Design Concept

Figure 1 illustrates the origin and design concept of the implant model. Inspired by the natural flexible periodontal membrane (see Figure 1a). The natural tooth root was observed by oral X-light machine (Carestream health Inc., NY) in department of stomatology, affiliated Hangzhou first people's hospital at the root–alveolar bone interface, which acts as a cushion during occlusion, this study addresses the limitations of current clinical implant designs. Traditional dental implants typically adopt a rigid bolt-like mechanical locking mechanism to connect with the alveolar bone (see Figure 1b, connection between artificial implant and alveolar bone was observed by oral X-light machine). This type of connection is prone to causing microfractures at the implant–bone interface under occlusal forces, thereby shortening the implant's service life. To overcome this issue, this paper proposes a biomimetic approach by designing a flexible structural layer on the implant surface that mimics the function of the periodontal membrane (see Figure 1c). The study further investigates and compares the mechanical properties of the implant interface before and after the introduction of this flexible layer.

2.2 | Finite Element Model Parameters of Flexible Composite-Coated Implant

The design parameters of the flexible composite-coated implant were primarily based on those of commercially available clinical implants and were developed using SolidWorks software. Figure 2 illustrates the modelling and load configuration of flexible composite-coated implant, cortical bone and cancellous bone. The structural parameters of the implant were referenced from the standard Swiss ITI implant, with the following specifications: bottom diameter $D = 4$ mm, implant length $L = 10$ mm, trapezoidal thread shape, thread height $d = 0.70$ mm, bottom thread width tw = 0.35 mm, pitch $p = 1.40$ mm, and thread angle $\theta = 60°$ (see Figure 2a). The thickness of the periodontal ligament (PDL) is patient-specific. Clinical studies indicate that the reference range for PDL thickness is typically between 0.15 and 0.38 mm [25]. The coating designed in this study serves as a biomimetic substitute for the PDL. Considering its future clinical value, a core requirement is that it should not alter the original structure of the standard clinical implant. The maximum allowable coating thickness is approximately 0.125 mm (exceeding this limit would change the trapezoidal thread profile to a V-shape, which is inconsistent with the isosceles trapezoidal

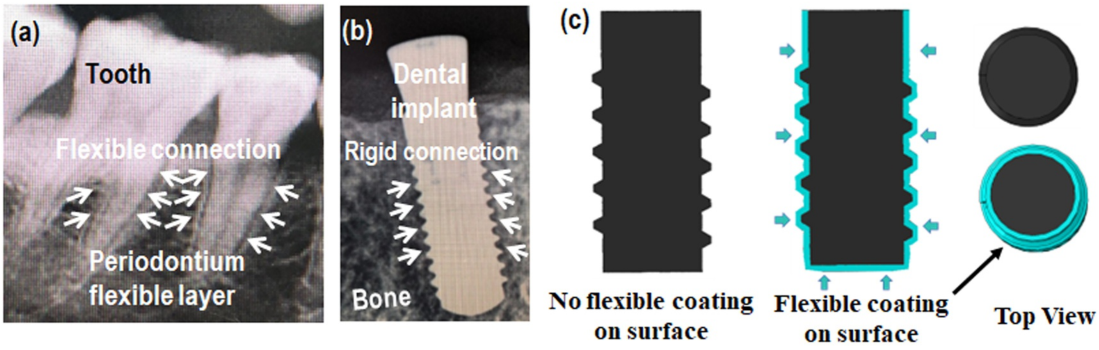

FIGURE 1 | Implant model source and design rationale. X-ray image of the connection between (a) nature tooth, (b) implant and the alveolar bone; (c) schematic diagram comparing the implant surface before and after the deposition of a flexible composite coating.

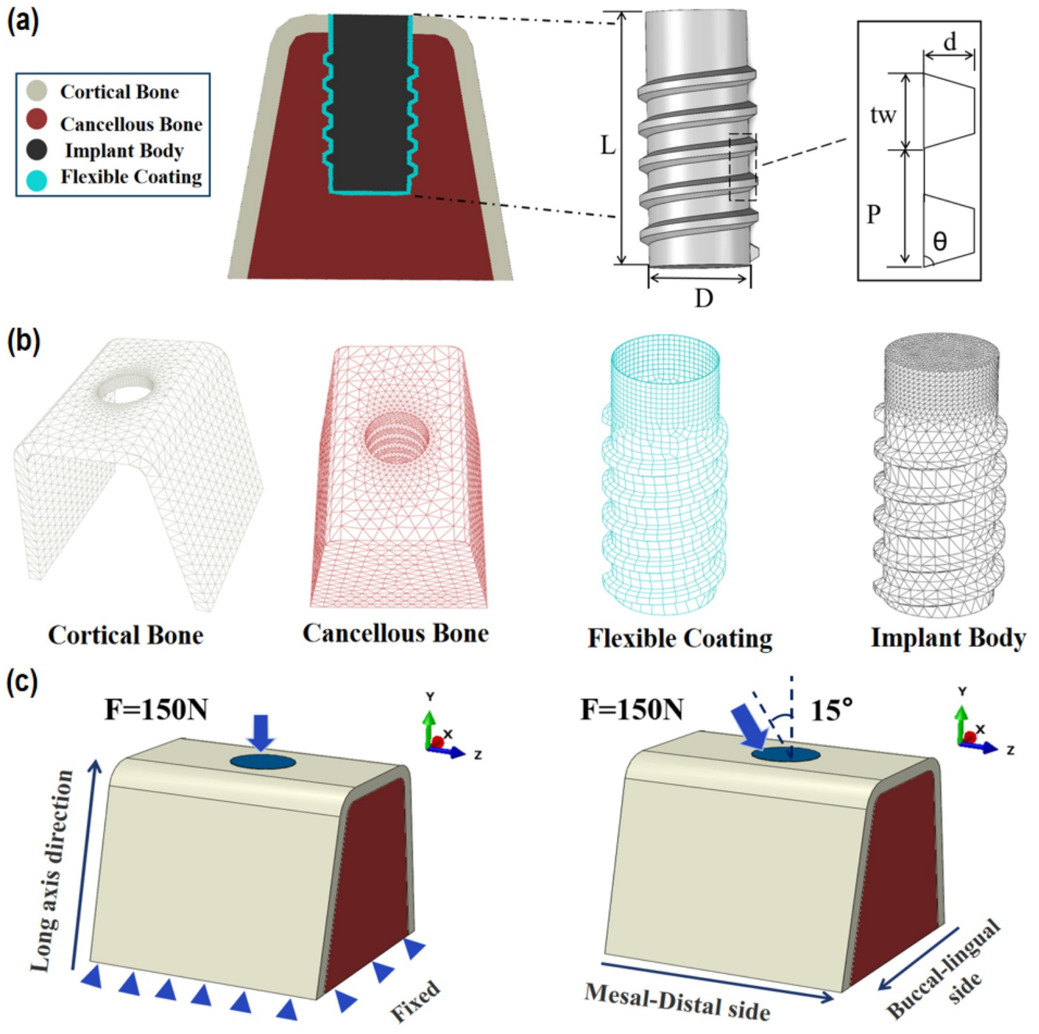

FIGURE 2 | Modelling and load configuration of flexible composite-coated implant, cortical bone, and cancellous bone. (a) ross-sectional view of the implant system assembly; (b) meshing diagram of cortical bone, cancellous bone, implant, and coating; (c) schematic diagram of load constraints.

structure of standard clinical implants). To expand the experimental variables and facilitate group design, this study preliminarily determined the structural layer thickness range to be 0.025–0.125 mm through finite element simulation. In this study, the application of the flexible composite coating on the implant surface was parameterised under two distinct conditions: (1) flexible composite-coated implant type I (simplified as FCCIT I): The flexible coating was applied directly onto the existing clinical implant parameters without altering the original thread structure. Coating thicknesses of 0.025 mm, 0.050 mm, 0.075 mm, 0.100 mm and 0.125 mm were added within the allowable range for coating application. (2) Flexible composite-coated implant type II (simplified as FCCIT II): The overall dimensions of the clinical implant were maintained unchanged. This was achieved by first proportionally thinning the metal substrate by 0.025 mm, 0.050 mm, 0.075 mm, 0.100 mm and 0.125 mm, respectively, and then applying the coating such that the final coated implant dimensions conformed to the standard parameters. Furthermore, alveolar bone density is one of the core determinants for the success of dental implant surgery. It directly affects the initial stability of the implant, osseointegration outcomes, surgical difficulty and long-term restoration success rates, and is determined by the ratio of bone minerals (hydroxyapatite) to bone matrix (collagen fibres). In clinical practice, bone density is broadly classified into four types: Dense bone (D_1), which consists entirely of cortical bone; thick cortical bone with fine cancellous bone (D_2); thin cortical bone with coarse cancellous bone (D_3) and cancellous bone (D_4), which consists entirely of cancellous bone. In clinical practice, D_2-type bone is commonly regarded as the ideal condition for implantation [26–28]. Therefore, this study adopts the standard D_2 bone type, with the cortical bone thickness set at 1 mm and the interior composed of cancellous bone (see Figure 2b).

2.3 | Material Properties and Mesh Generation

The assembly model from SolidWorks was imported into Abaqus in.x_t format. The imported model was then inspected and optimised to ensure accuracy. Material properties assigned to all components were assumed to be linear elastic, homogeneous, and isotropic. Relevant mechanical parameters are listed in Table 1 [27, 29], with the following values: (1) implant (assumed to be Ti-6Al-4V alloy): elastic modulus = 115 GPa, Poisson's ratio = 0.35; (2) cortical bone: elastic modulus = 13.7 GPa, Poisson's ratio = 0.3; (3) cancellous bone: elastic modulus = 1.37 GPa, Poisson's ratio = 0.3 and (4) flexible composite coating (assumed to be a homogeneous, single-layered, polymer-based structure): elastic modulus = 2.0 GPa, Poisson's ratio = 0.3. Mesh quality and type influence simulation accuracy. To balance computational efficiency and precision, localised mesh refinement was applied, and a mesh independence verification was performed. A global mesh size of 1 mm was set for the cortical bone and cancellous bone edges. Regions such as the cancellous bone socket in direct contact with the implant, implant threads and flexible composite coating structure were refined. The mesh size at the implant and flexible composite coating threads was set to 0.5 mm, whereas the cortical bone at the implant neck and the cancellous bone socket were refined to 0.2 mm. For the two flexible composite coating designs, FCCIT I and FCCIT II, the total number of elements in the models ranged from 95,676 to 112,096, and the number of nodes ranged from 19,503 to 24,020. Regarding element selection: The flexible composite coating was meshed with S4R elements. S4R is a 4-node reduced integration quadrilateral shell element suitable for thin-walled structures such as coatings; it offers high computational efficiency and effectively avoids shear locking, accurately reflecting the bending and deformation behaviour of the flexible layer under load. All other components were meshed with C3D4 elements. C3D4 is a 4-node linear tetrahedral solid element ideal for complex three-dimensional solids (implant body, cancellous bone and intricate thread structures); it provides strong adaptability to irregular geometries and is widely used in biomedical finite element analysis. The flexible composite coating was meshed with S4R elements, whereas all other components were meshed with C3D4 elements.

TABLE 1 | Materials properties of implant components.

Materials	Implant	Cortical bone	Cancellous bone	Flexible coating
Elastic modulus (GPa)	115	13.7	1.37	2.0
Poisson's ratio	0.35	0.3	0.3	0.3

2.4 | Contact Conditions and Load Configuration

Because the implant restoration model is an assembly with interaction relationships between components, contact conditions must be defined to transmit loads. All parts were assigned tie constraints, and the buccolingual and mesiodistal sides of the cancellous bone were set as fully fixed [28–30]. Oral biting force is influenced by factors such as masticatory muscle strength, dental and periodontal condition, age and chewing habits. Bite force magnitude gradually decreases from the molar region to the premolar and anterior regions. The molar region primarily bears vertical axial loads, corresponding to direct up-and-down chewing in the posterior area. In contrast, the premolar and anterior regions mainly experience horizontal and lateral forces, as food tends to shift laterally during chewing, resulting in lateral loads within an approximate angular range of 0°–45° [31]. Substantial data indicate that the maximum bite force of a healthy adult's unilateral molar ranges from 300 to 600 N, whereas the functional occlusal force during daily chewing is only 15%–30% of the maximum bite force [32, 33]. Multiple studies have adopted an average adult biting force of 150 N as the load magnitude [27, 34]. The direction of the biting force is primarily vertical (perpendicular to the occlusal plane), corresponding to straight up-and-down chewing in the posterior region. A common angular range considered is 0° ± 30° (including horizontal and lateral components), varying with chewing position and phase. For unilateral chewing, an average deviation angle of 15° was selected to simulate food-induced lateral offset [30]. Accordingly, this study applied a load of 150 N under two loading conditions: vertical and oblique. The oblique load was applied at a 15° angle to the *y*-axis within the *y*–*x* plane (see Figure 2c).

2.5 | Observational Index

The primary observation focuses on the mechanical properties of the implant–bone interface in each group of models before and after coating addition, specifically the Von Mises equivalent stress and strain between the implant and the alveolar bone. Von Mises stress serves as a key indicator for evaluating the mechanical stability of the interface. After implant placement, the interface is subjected to complex loads such as occlusal forces and lateral forces, resulting in three-dimensional stress. The calculation formula is as follows:

$$\sigma_{vm} = \sqrt{\frac{1}{2}(\sigma_1 - \sigma_2)^2 + (\sigma_2 - \sigma_3)^2 + (\sigma_3 - \sigma_1)^2},$$

where σ_1, σ_2 and σ_3 represent the principal stresses. Based on the cloud distribution of the components, the peak values of equivalent stress and strain were recorded to compare the effects before and after coating addition, as well as the influence of thickness variations on the models. The yield strength of cortical bone is 140–170 MPa, whereas that of cancellous bone is 22–28 MPa [35]. Exceeding these values may lead to irreversible structural damage.

3 | Results and Discussion

3.1 | Analysis of the Mechanical Properties of FCCIT I Implant Under a Vertical Load

Figure 3 shows the stress distribution at the implant–bone interface of FCCIT I implant with flexible composite coating under vertical loads with varying coating thicknesses. Figure 3a,b display the stress distribution nephograms of the flexible composite coating on the implant surface with thicknesses of 0, 0.025, 0.050, 0.075, 0.100 and 0.125 mm under vertical loading. The corresponding maximum peak stresses are 20.2, 13.5, 13.5, 13.1, 12.7 and 13.2 MPa, respectively. The results indicate that after adding the flexible composite coating to the implant surface, the peak stress under the same load notably decreased by up to approximately 37%. However, variations in the thickness of the flexible composite coating from 0.025 to 0.125 mm did not apparently affect the implant stress. Figure 3c,d present the stress distribution nephograms of the alveolar bone after adding flexible composite coatings of different thicknesses to the implant surface. The results show that after applying the flexible composite coating to the implant, the peak stress in the alveolar bone also exhibited a decreasing trend, with a maximum reduction of approximately 22%. Nevertheless, the peak stress in the alveolar bone demonstrated a certain sensitivity to the thickness of the flexible composite coating on the implant. Specifically, when the coating thickness increased from 0.025 to 0.05 mm, the peak stress in the alveolar bone showed an increasing trend. As the coating thickness increased from 0.05 to 0.075 mm, the peak stress stabilised. Finally, when the coating thickness increased from 0.075 to 0.125 mm, the peak stress first decreased and then slightly increased.

Figure 4 shows the strain distribution at the implant–bone interface of FCCIT I implant with flexible composite coating under vertical loads with varying coating thicknesses. Figure 4a,b display the strain distribution nephograms of the flexible composite coating on the implant surface with thicknesses of 0 mm, 0.025 mm, 0.050 mm, 0.075 mm, 0.100 mm and 0.125 mm under vertical loading. The corresponding maximum peak strains are 9.8×10^{-5}, 5.8×10^{-5}, 5.7×10^{-5}, 5.8×10^{-5}, 5.3×10^{-5} and 6.2×10^{-5}, respectively. The results indicate that after adding the flexible composite coating to the implant surface, the peak strain under the same load notably decreased by up to approximately 46%. However, variations in the coating thickness from 0.025 to 0.125 mm did not apparently affect the implant strain. Figure 4c,d present the strain distribution nephograms of the alveolar bone after adding flexible composite coatings of different thicknesses to the implant surface. The results show that after applying the flexible composite coating to the implant, no apparent trend was observed in the change of peak strain in the alveolar bone before and after the coating addition.

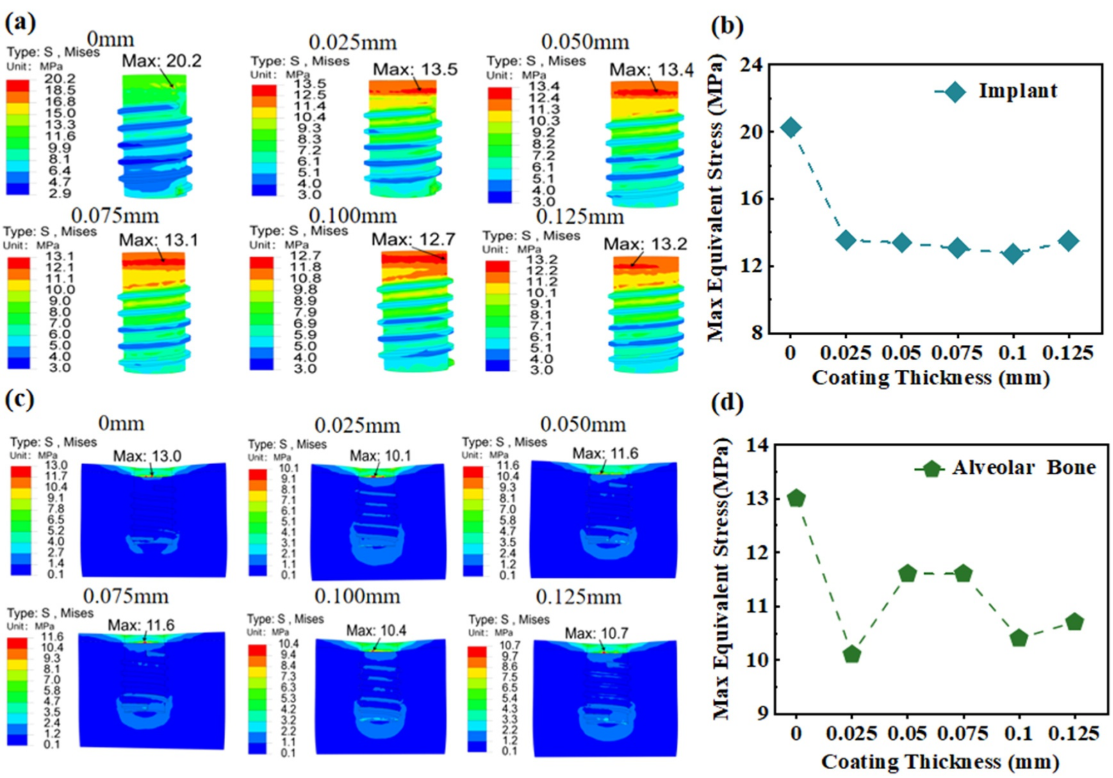

FIGURE 3 | Stress distribution at the implant–bone interface of FCCIT I implant with flexible composite coating under vertical loads with varying coating thicknesses. (a) Stress distribution in the FCCIT I implant; (b) variation of maximum stress in the FCCIT I implant with different flexible composite coating thicknesses; (c) stress distribution in the alveolar bone; (d) variation of maximum stress in the alveolar bone with different flexible composite coating thicknesses.

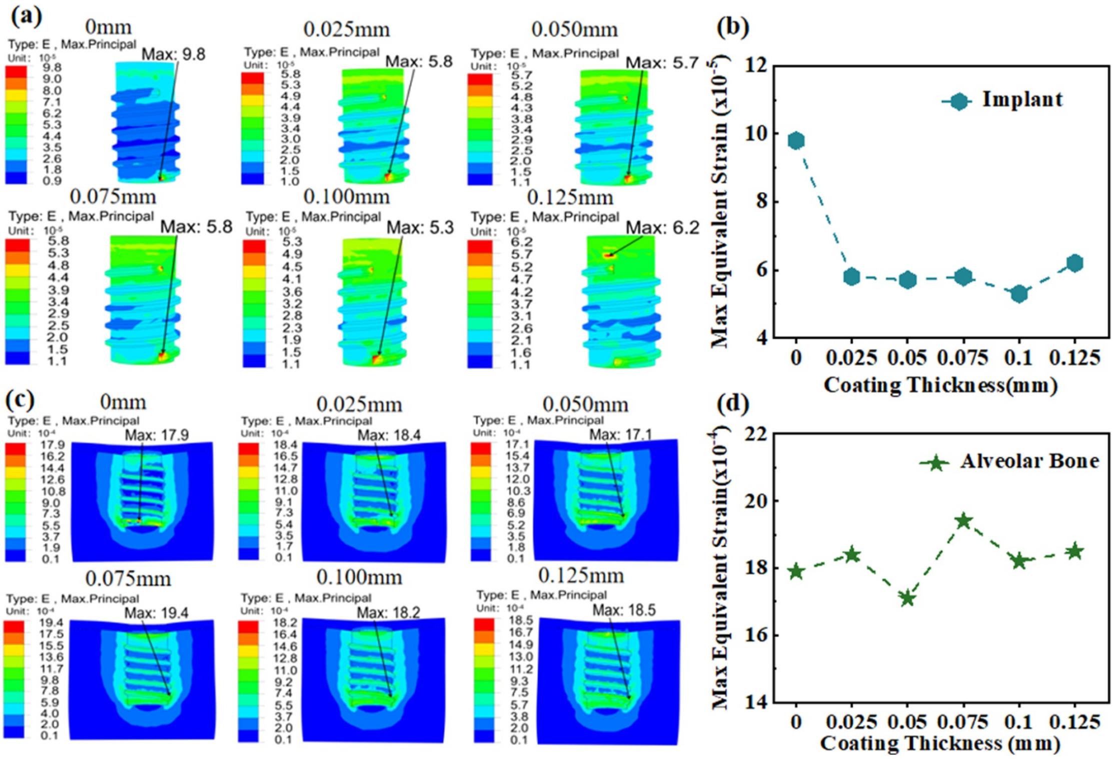

FIGURE 4 | Strain distribution at the implant–bone interface of FCCIT I implant with flexible composite coating under vertical loads with varying coating thicknesses. (a) Strain distribution in the FCCIT I implant; (b) variation of maximum strain in the FCCIT I implant with different flexible composite coating thicknesses; (c) strain distribution in the alveolar bone; (d) variation of maximum strain in the alveolar bone with different flexible composite coating thicknesses.

3.2 | Analysis of the Mechanical Properties of FCCIT I Implant Under a 15° Inclination Load

Figure 5 illustrates the stress distribution at the implant–bone interface of FCCIT I implant with flexible composite coating under a 15° inclination load with varying coating thicknesses. Figure 5a,b display the stress distribution nephograms of the flexible composite coating on the implant surface with thicknesses of 0, 0.025, 0.050, 0.075, 0.100 and 0.125 mm under a 15° inclination load. The corresponding maximum peak stresses are 65.8 MPa, 56.6 MPa, 59.9 MPa, 57.9 MPa, 57.7 MPa and 54.8 MPa, respectively. The results indicate that after adding the flexible composite coating to the implant surface, the peak stress under the same inclined load significantly decreased by up to approximately 16.7%. However, variations in the coating thickness from 0.025 to 0.125 mm did not significantly affect the implant stress. Figure 5c,d present the stress distribution nephograms of the alveolar bone after adding flexible composite coatings of different thicknesses to the implant surface. The results show that after applying the flexible composite coating to the implant, the peak stress in the alveolar bone also exhibited a decreasing trend, with a maximum reduction of approximately 30.6%. Furthermore, the peak stress in the alveolar bone did not exhibit sensitivity to the thickness of the flexible composite coating added to the implant.

Figure 6 illustrates the strain distribution at the implant–bone interface of FCCIT I implant with flexible composite coating under a 15° inclination load with varying coating thicknesses. Figure 6a,b respectively show the strain distribution nephograms of the flexible composite coating on the implant surface with thicknesses of 0, 0.025, 0.050, 0.075, 0.100 and 0.125 mm under a 15° inclination load. The corresponding maximum peak strains are 59.0 $\times$ 10^{-5}, 35.6 $\times$ 10^{-5}, 46.6 $\times$ 10^{-5}, 38.5 $\times$ 10^{-5}, 37.5 $\times$ 10^{-5} and 31.8 $\times$ 10^{-5}. The results indicate that after adding the flexible composite coating to the implant surface, the peak strain under the same load significantly decreased by up to approximately 46%. Excluding the 0.05 mm thickness, variations in the coating thickness from 0.025 to 0.125 mm did not significantly affect the implant strain. Figure 6c,d present the strain distribution nephograms of the alveolar bone after adding flexible composite coatings of different thicknesses to the implant surface. The results show that after applying the flexible composite coating to the implant, excluding the 0.075 mm thickness, the peak strain in the alveolar bone exhibited a decreasing trend as the thickness of the flexible composite coating increased.

3.3 | Analysis of the Mechanical Properties of FCCIT II Implant Under a Vertical Load

Figure 7 shows the stress distribution at the implant–bone interface of FCCIT II implant with flexible composite coating under vertical loads with varying coating thicknesses. Figure 7a,b respectively display the stress distribution nephograms of the flexible composite coating on the implant surface with thicknesses of 0, 0.025, 0.050, 0.075, 0.100 and 0.125 mm under vertical loading. The corresponding maximum peak stresses are 20.2 MPa, 13.9 MPa, 13.7 MPa, 13.8 MPa, 14.6 MPa

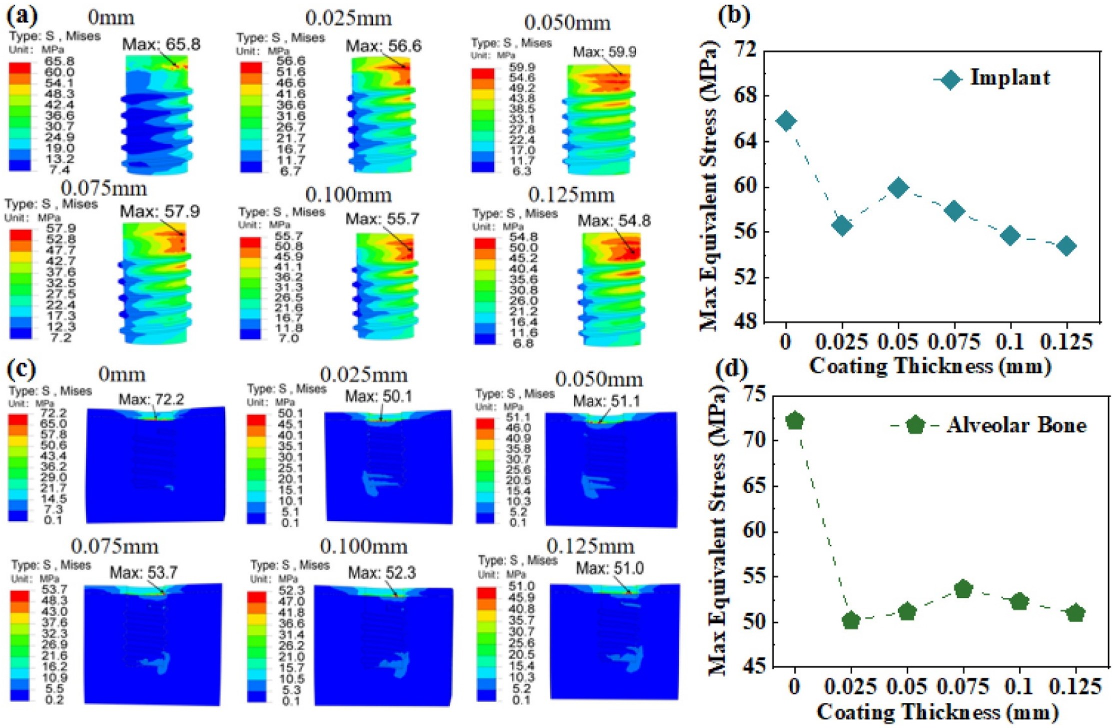

FIGURE 5 | Stress distribution at the implant–bone interface of FCCIT I implant with flexible composite coating under a 15° inclination load with varying coating thicknesses. (a) Stress distribution in the FCCIT I implant; (b) variation of maximum stress in the FCCIT I implant with different flexible composite coating thicknesses; (c) stress distribution in the alveolar bone; (d) variation of maximum stress in the alveolar bone with different flexible composite coating thicknesses.

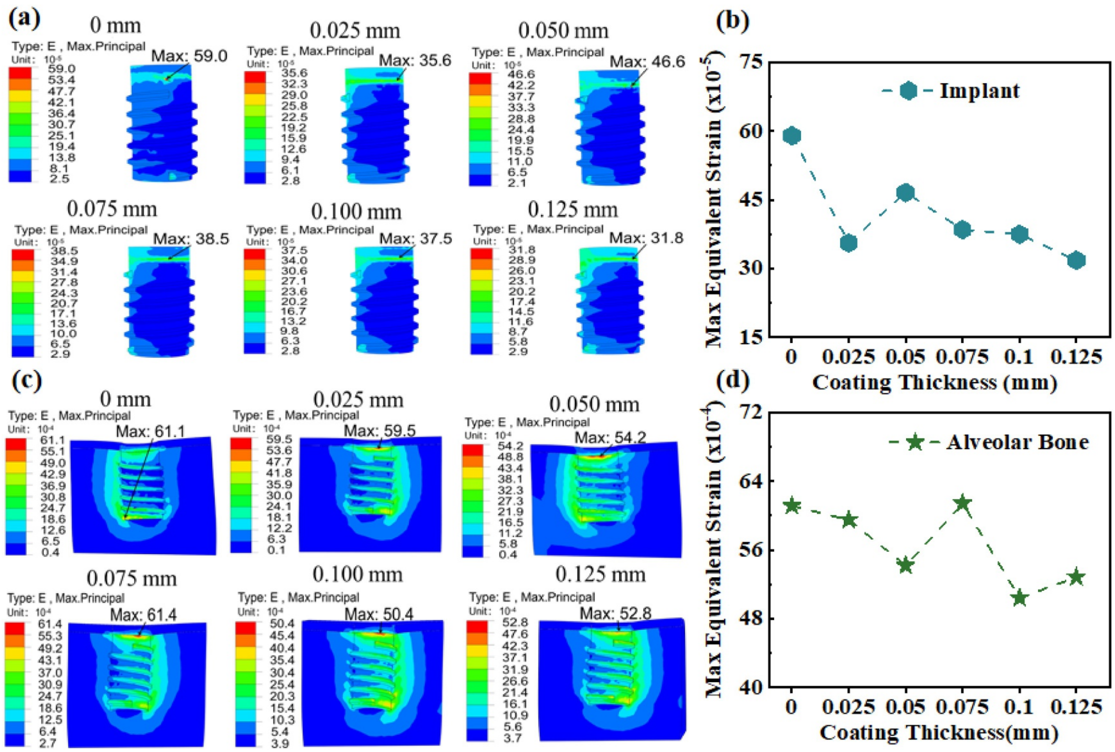

FIGURE 6 | Strain distribution at the implant–bone interface of FCCIT I implant with flexible composite coating under a 15° inclination load with varying coating thicknesses. (a) Strain distribution in the FCCIT I implant; (b) variation of maximum strain in the FCCIT I implant with different flexible composite coating thicknesses; (c) strain distribution in the alveolar bone; (d) variation of maximum strain in the alveolar bone with different flexible composite coating thicknesses.

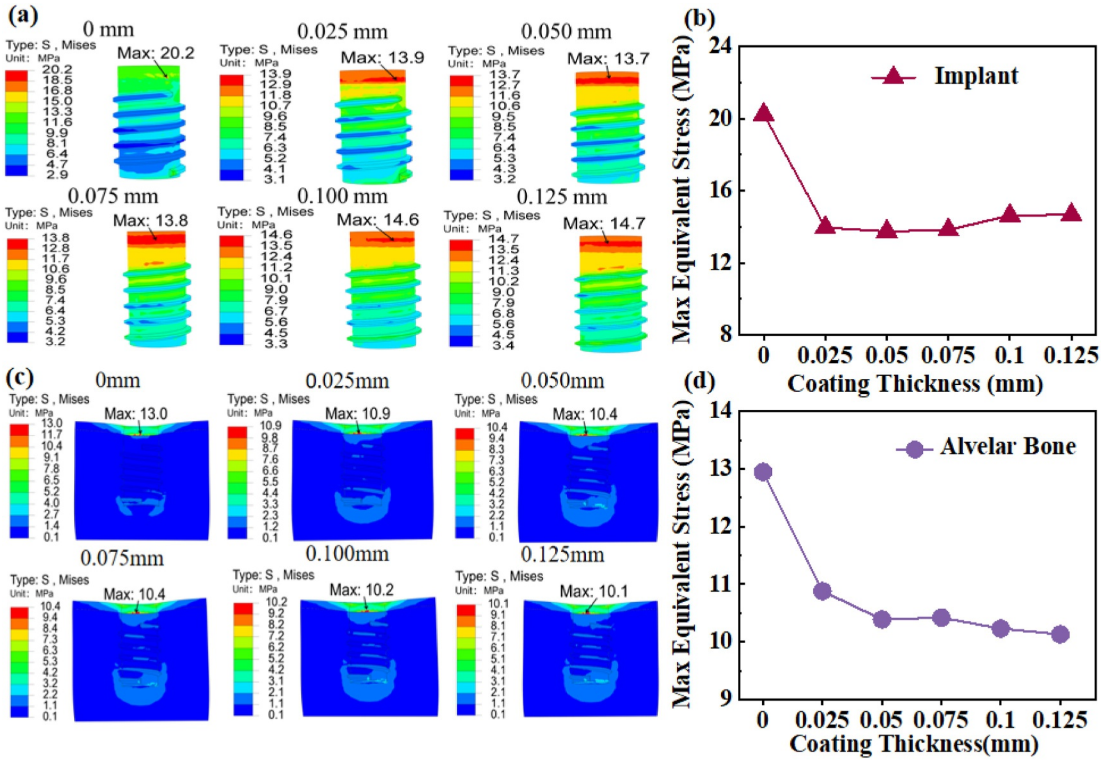

FIGURE 7 | Stress distribution at the implant–bone interface of FCCIT II implant with flexible composite coating under vertical loads with varying coating thicknesses. (a) Stress distribution in the FCCIT II implant; (b) variation of maximum stress in the FCCIT II implant with different flexible composite coating thicknesses; (c) stress distribution in the alveolar bone; (d) variation of maximum stress in the alveolar bone with different flexible composite coating thicknesses.

and 14.7 MPa. The results indicate that after adding the flexible composite coating to the implant surface, the peak stress under the same load significantly decreased by up to approximately 32.2%. However, variations in the coating thickness from 0.025 to 0.125 mm did not significantly affect the implant stress. Figure 7c,d present the stress distribution nephograms of the alveolar bone after adding flexible composite coatings of different thicknesses to the implant surface. The results show that after applying the flexible composite coating to the implant, the peak stress in the alveolar bone also exhibited a decreasing trend, with a maximum reduction of approximately 22.3%.

Figure 8 shows the strain distribution at the implant–bone interface of FCCIT II implant with flexible composite coating under vertical loads with varying coating thicknesses. Figure 8a,b respectively display the strain distribution nephograms of the flexible composite coating on the implant surface with thicknesses of 0, 0.025, 0.050, 0.075, 0.100 and 0.125 mm under vertical loading. The corresponding maximum peak strains are 9.8×10^{-5}, 5.5×10^{-5}, 5.5×10^{-5}, 6.1×10^{-5}, 7.1×10^{-5} and 8.7×10^{-5}. The results indicate that after adding the flexible composite coating to the implant surface, the peak strain under the same load significantly decreased by up to approximately 44%. However, as the thickness of the flexible composite coating increased, the implant strain exhibited an upward trend. Figure 8c,d present the strain distribution nephograms of the alveolar bone after adding flexible composite coatings of different thicknesses to the implant surface. The results show that after applying the flexible composite coating to the implant, the peak strain in the alveolar bone demonstrated a certain sensitivity to the coating application. Excluding the 0.05 mm thickness, the peak strain in the alveolar bone showed an increasing trend with the addition of the flexible composite coating.

3.4 | Analysis of the Mechanical Properties of FCCIT II Implant Under a 15° Inclination Load

Figure 9 illustrates the stress distribution at the implant–bone interface of FCCIT I implant with flexible composite coating under a 15° inclination load with varying coating thicknesses. Figure 9a,b respectively display the stress distribution nephograms of the flexible composite coating on the implant surface with thicknesses of 0, 0.025, 0.050, 0.075, 0.100 and 0.125 mm under a 15° inclination load. The corresponding maximum peak stresses are 65.8 MPa, 55.7 MPa, 53.5 MPa, 52.8 MPa, 54.0 MPa and 54.5 MPa. The results indicate that after adding the flexible composite coating to the implant surface, the peak stress under the same inclined load significantly decreased by up to approximately 19.8%. However, variations in the coating thickness from 0.025 to 0.125 mm did not significantly affect the stress change. Figure 9c,d present the stress distribution nephograms of the alveolar bone after adding flexible composite coatings of different thicknesses to the implant surface. The results show that after applying the flexible composite coating to the implant, the peak stress in the alveolar bone also exhibited a decreasing trend, with a maximum reduction of approximately 35%. Furthermore, as the thickness of the flexible composite coating on the implant increased from 0.025 to 0.125 mm, the peak stress in the alveolar bone showed a decreasing trend.

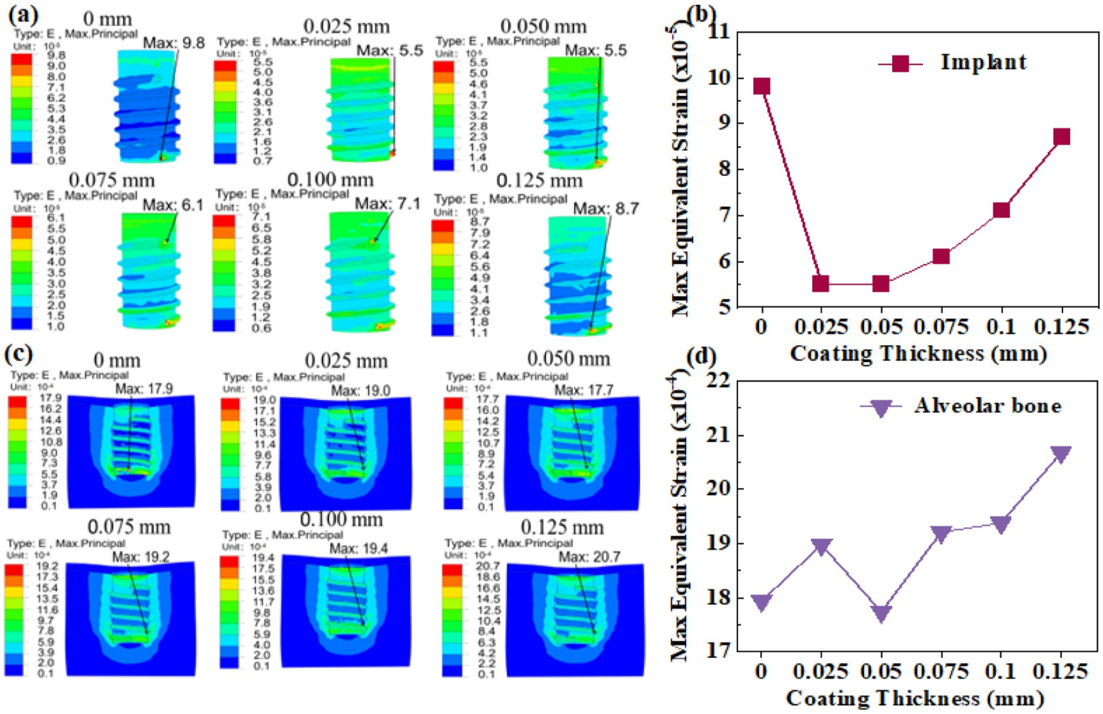

FIGURE 8 | Strain distribution at the implant–bone interface of FCCIT II implant with flexible composite coating under vertical loads with varying coating thicknesses. (a) Strain distribution in the FCCIT II implant; (b) variation of maximum strain in the FCCIT II implant with different flexible composite coating thicknesses; (c) strain distribution in the alveolar bone; (d) variation of maximum strain in the alveolar bone with different flexible composite coating thicknesses.

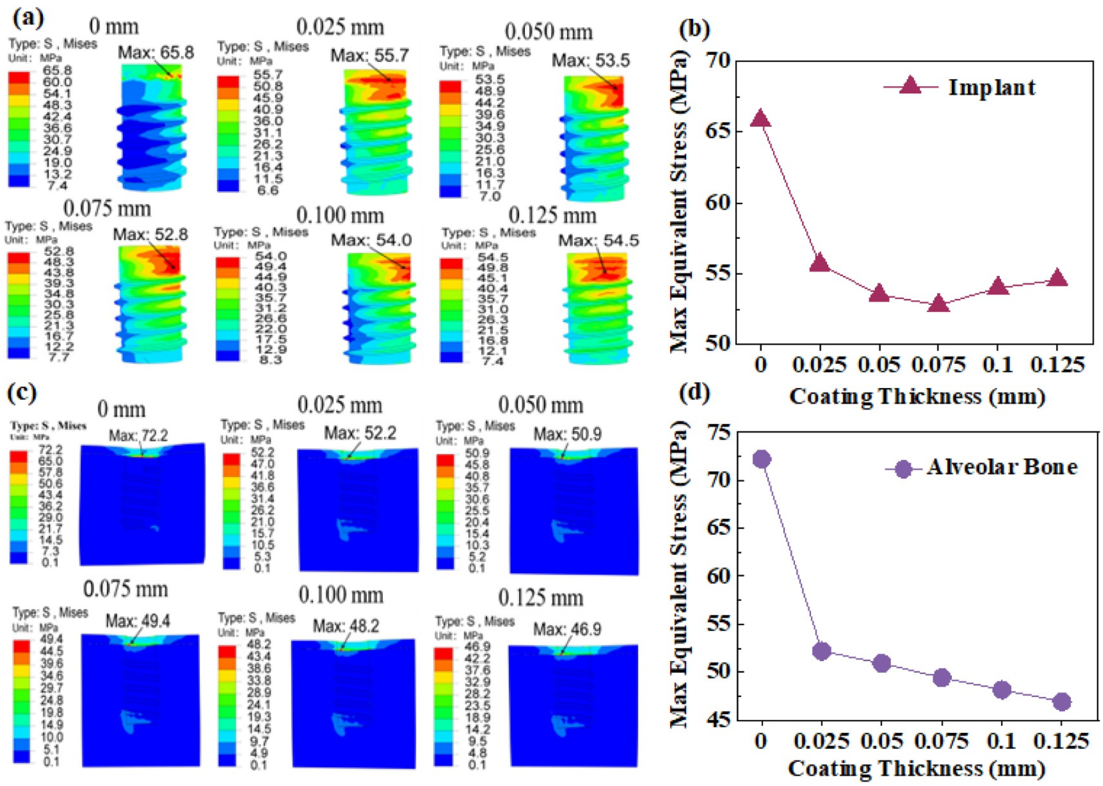

FIGURE 9 | Stress distribution at the implant–bone interface of FCCIT II implant with flexible composite coating under a 15° inclination load with varying coating thicknesses. (a) Stress distribution in the FCCIT II implant; (b) variation of maximum stress in the FCCIT II implant with different flexible composite coating thicknesses; (c) stress distribution in the alveolar bone; (d) variation of maximum stress in the alveolar bone with different flexible composite coating thicknesses.

Figure 10 illustrates the strain distribution at the implant–bone interface of FCCIT II implant with flexible composite coating under a 15° inclination load with varying coating thicknesses. Figure 10a,b respectively display the strain distribution nephograms of the flexible composite coating on the implant surface with thicknesses of 0, 0.025, 0.050, 0.075, 0.100 and 0.125 mm under a 15° inclination load. The corresponding maximum peak strains are 59.0×10^{-5}, 28.4×10^{-5}, 31.9×10^{-5}, 31.6×10^{-5}, 31.1×10^{-5} and 27.7×10^{-5}. The results indicate that after adding the flexible composite coating to the implant surface, the peak strain under the same load significantly decreased by up to approximately 53%. However, variations in the coating thickness did not significantly affect the implant strain. Figure 10c,d present the strain distribution nephograms of the alveolar bone after adding flexible composite coatings of different thicknesses to the implant surface. The results show that after applying the flexible composite coating to the implant, the peak strain in the alveolar bone increased (except for the 0.05 mm thickness).

3.5 | Comparison of the Effects of Addition Methods of Flexible Composite Coatings Under a Vertical Load

By comparing the peak stress and strain of the implant and alveolar bone under vertical load after applying different flexible composite coating addition methods, it is shown that the method of adding flexible composite coatings has a certain impact on the mechanical properties of the implant–alveolar bone interface. Figure 11 presents the variation diagrams of the peak equivalent stress and strain for the implant and alveolar bone under vertical load using two flexible composite coating addition methods: FCCIT I and FCCIT II. Figure 11a compares the peak stress variation of the implant under the FCCIT I and FCCIT II coating addition methods. It shows that within the coating thickness range of 0.025–0.125 mm, the percentage decrease in equivalent stress for the FCCIT I method is consistently higher than that for the FCCIT II method. The largest difference between the two occurs at 0.100 mm, approximately 9.35%. Figure 11b compares the peak stress variation of the alveolar bone under the FCCIT I and FCCIT II coating addition methods. It indicates that only at a coating thickness of 0.025 mm does the FCCIT I method result in a greater percentage stress reduction compared to the FCCIT II method. From 0.05 to 0.125 mm coating thickness, the percentage decrease in equivalent stress for the FCCIT I method is lower than that for the FCCIT II method, with the largest difference occurring at 0.075 mm, approximately 9.22%. Figure 11c compares the peak strain variation of the implant under the FCCIT I and FCCIT II coating addition methods. It reveals that the difference between the FCCIT I and FCCIT II methods is minimal at thicknesses ranging from 0.025 to 0.075 mm. However, from 0.100 to 0.125 mm, the percentage decrease in equivalent strain for the FCCIT I method becomes more significant, with the maximum difference reaching up to 25.5%. Figure 11d compares the peak strain variation of the alveolar bone under the FCCIT I and FCCIT II coating addition methods. It demonstrates that the impact of the two flexible composite coating addition methods on alveolar bone strain is neither consistent nor significant. In

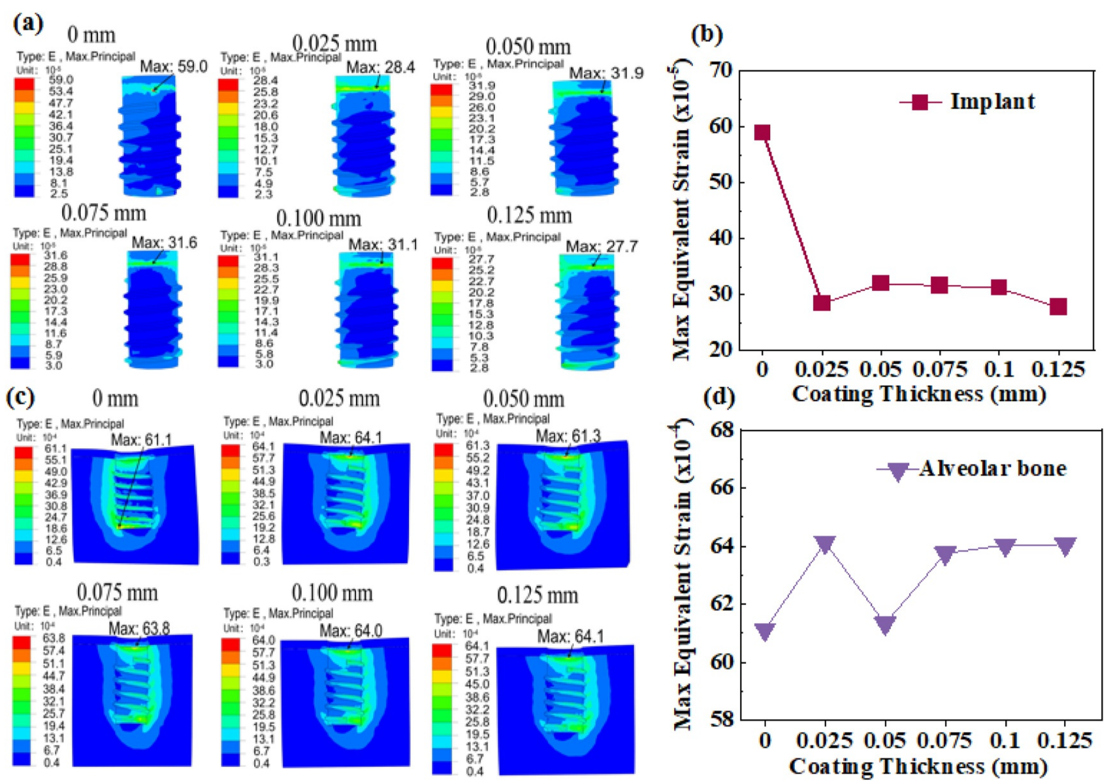

FIGURE 10 | Strain distribution at the implant–bone interface of FCCIT II implant with flexible composite coating under a 15° inclination load with varying coating thicknesses. (a) Strain distribution in the FCCIT II implant; (b) variation of maximum strain in the FCCIT II implant with different flexible composite coating thicknesses; (c) strain distribution in the alveolar bone; (d) variation of maximum strain in the alveolar bone with different flexible composite coating thicknesses.

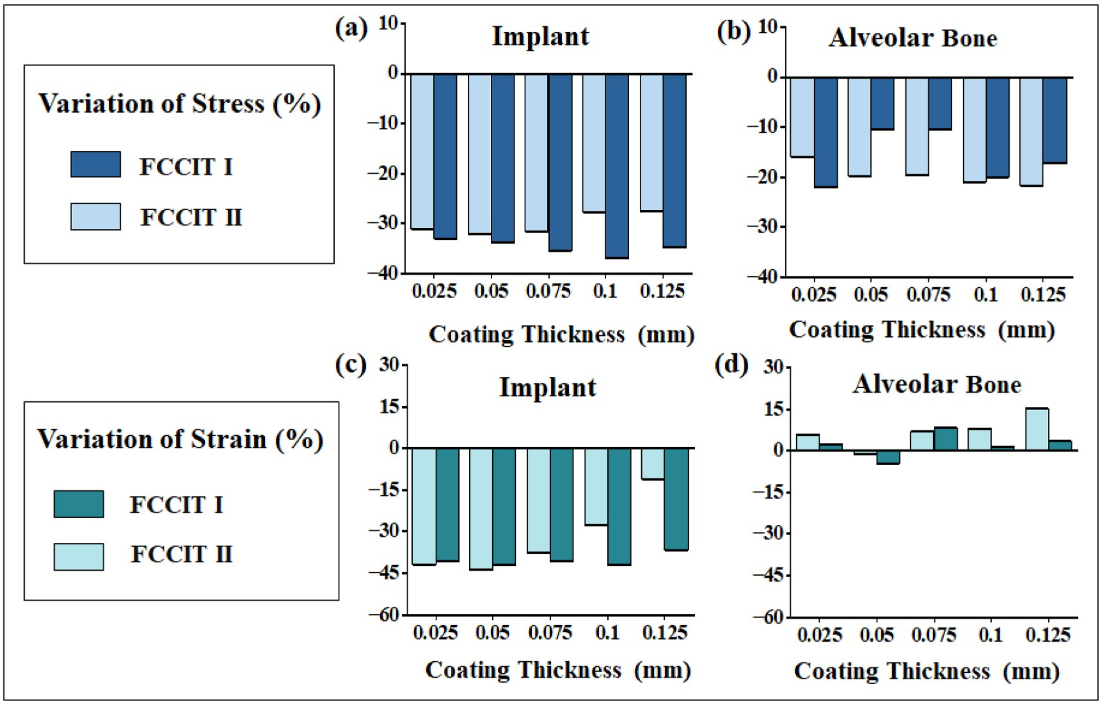

FIGURE 11 | Variation in stress and strain peaks between the implant and alveolar bone for FCCIT I and FCCIT II type implants with flexible composite coating addition under vertical loading. Stress variation in (a) the implant and (b) the alveolar bone; strain variation in (a) the implant and (b) the alveolar bone.

summary, the FCCIT I flexible composite coating addition method generally exhibits superior ability in buffering vertical loads compared to the FCCIT II method.

3.6 | Comparison of the Effects of Addition Methods of Flexible Composite Coatings Under a 15° Inclination Load

Figure 12 presents the variation diagrams of the peak equivalent stress and strain for the implant and alveolar bone under a 15° inclination load using two flexible composite coating addition methods: FCCIT I and FCCIT II. Figure 12a compares the peak stress variation of the implant under the FCCIT I and FCCIT II coating addition methods. Within the coating thickness range of 0.025–0.125 mm, the percentage decrease in equivalent stress for the FCCIT II method is consistently higher than that for the FCCIT I method. The difference is most significant during the thickness change from 0.05 to 0.075 mm, reaching a maximum of 9.72%. Figure 12b compares the peak stress variation of the alveolar bone under the FCCIT I and FCCIT II coating addition methods. It shows that only at a coating thickness of 0.025 mm does the FCCIT I method result in a greater percentage stress reduction compared to the FCCIT II method. The difference is minimal at a thickness of 0.05 mm. From 0.075 to 0.125 mm coating thickness, the percentage decrease in equivalent stress for the FCCIT I method is lower than that for the FCCIT II method. Figure 12c compares the peak strain variation of the implant under the FCCIT I and FCCIT II coating addition methods. It indicates that the FCCIT II method has a greater impact on the equivalent strain of the implant. The largest difference between the two methods occurs at a thickness of 0.05 mm, approximately 24.9%. Figure 12d compares the peak strain variation of the alveolar bone under the FCCIT I and FCCIT II coating addition methods. It shows that for the FCCIT I method, the strain decreases at all thicknesses except 0.075 mm, whereas for the FCCIT II method, the strain increases after adding the flexible composite coating across all thicknesses. In summary, the FCCIT II flexible composite coating addition method generally exhibits superior ability in buffering inclined loads compared to the FCCIT I method.

The current study primarily employed static loading conditions. To more accurately simulate the dynamic nature of oral masticatory function, future model modifications could incorporate dynamic loading profiles. This would involve defining time-dependent load functions within the FEA software to simulate the complete progression of occlusal force from onset to peak and dissipation during a chewing cycle (approximately 0.8–1.2 s). For instance, a peak load of 150 N could be applied with superimposed horizontal and lateral components (e.g., 5–10 N) to replicate the effect of food-induced lateral deviation during mastication. Furthermore, the model's boundary conditions could be adjusted to better reflect load transmission characteristics at different implant sites. Posterior implants predominantly experience vertical loads, thus retaining fully fixed constraints on the cancellous bone is appropriate. Conversely, anterior implants are subject to more pronounced horizontal and lateral force components; for such models, constraints in the horizontal direction could be partially relaxed to mimic the flexible cushioning of the natural periodontal ligament, thereby providing a more realistic simulation of the biomechanical environment in the anterior region. The distinct mechanical behaviours of FCCIT I and FCCIT II coatings suggest different potential clinical benefits. FCCIT I, which exhibited superior vertical load buffering, would be particularly advantageous for patients with normal occlusal relationships and primarily axial chewing

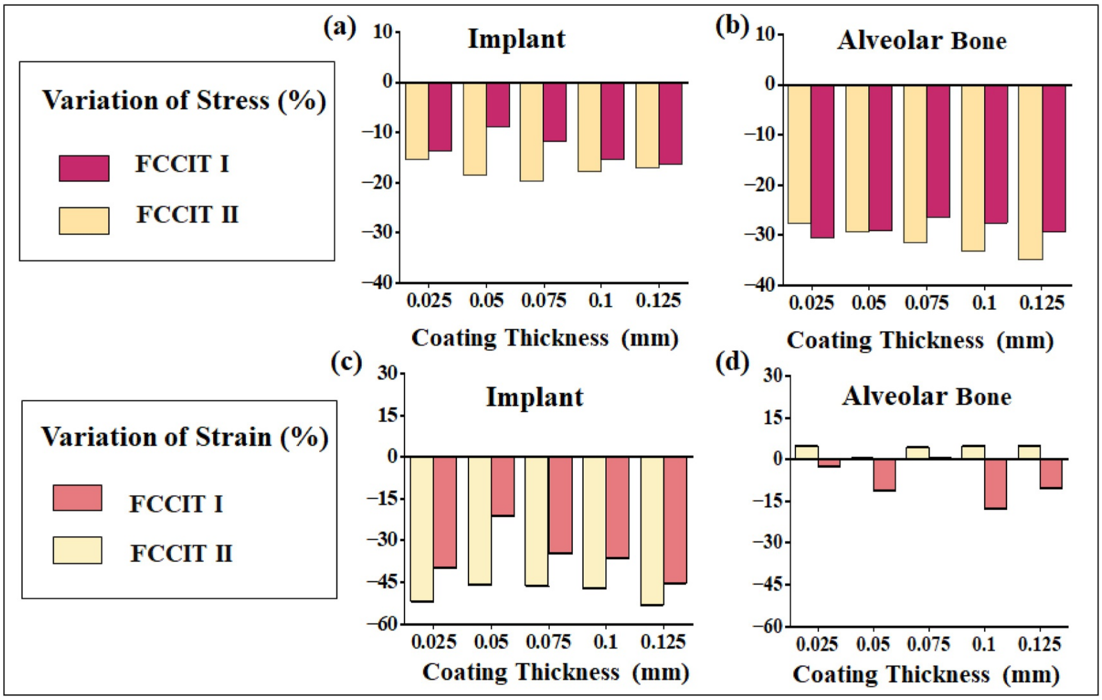

FIGURE 12 | Variation in stress and strain peaks between the implant and alveolar bone for FCCIT I and FCCIT II type implants with flexible composite coating addition under a 15° inclination loading. Stress variation in (a) the implant and (b) the alveolar bone; strain variation in (a) the implant and (b) the alveolar bone.

patterns. Vertical loads constitute over 60% of daily masticatory forces. The 0.100 mm thick FCCIT I coating reduced peak implant stress by up to 37.1%, which could effectively mitigate vertical stress concentration at the implant–bone interface, thereby reducing the risk of crestal bone resorption and subsequent implant loosening. In contrast, FCCIT II demonstrated superior capacity in buffering oblique loads, which are commonly encountered during lateral chewing, in patients with occlusal discrepancies, or in those with parafunctional habits such as bruxism. The 0.125 mm thick FCCIT II coating reduced peak equivalent stress in the alveolar bone by 35.0% and peak strain in the implant by 53.1% under inclined loading. This design could effectively disperse shear and torsional stresses around the implant, protecting the peri-implant bone tissue and mitigating damage to the implant thread structure, thereby extending the implant's service life.

4 | Conclusion

This study investigates the effects of adding a flexible composite coating to the implant surface by comparing the stress and strain changes at the implant–alveolar bone interface before and after coating application. The aim is to explore the impact of designing a flexible structural layer on the implant surface that mimics the periodontal ligament, providing theoretical guidance for the bionic design of implant surfaces resembling the periodontal ligament. Based on existing clinical implant structures, two flexible coating addition methods (FCCIT I and FCCIT II) were designed in this study. Through comparative analysis under vertical and 15° inclined loads, the following conclusions were drawn:

1. Both the FCCIT I and FCCIT II flexible composite coating addition methods can optimise stress distribution, reduce stress concentration and achieve load buffering. For the implant, stress is primarily transmitted to the first thread area, whereeas for the alveolar bone, stress is transmitted to the bottom and surrounding areas of the implant socket.
2. The FCCIT I flexible composite coating addition method generally exhibits superior ability in buffering vertical loads compared to FCCIT II.
3. The FCCIT II flexible composite coating addition method generally exhibits superior ability in buffering inclined loads compared to FCCIT I.

Acknowledgements

We gratefully acknowledge the support of the National Natural Science Foundation of China (Grant Nos. 52575214 and 52205198) for this study.

Conflicts of Interest

The authors declare no conflicts of interest.

Data Availability Statement

Data available on request from the authors.

References

1. C. V. Graves, S. K. Harrel, J. A. Rossmann, et al., “The Role of Occlusion in the Dental Implant and Peri-Implant Condition: A Review,” *Open Dentistry Journal* 10, no. 1 (2016): 594–601, https://doi.org/10.2174/1874210601610010594.

2. L. Shujie, L. Chan, T. Jiaqing, L. Yongwei, D. Hanlin, and L. Lihua, "Application of Implant-Supported Provisional Healing Abutments in Anterior Aesthetics," *International Dental Journal* 75 (2025): 105180, https://doi.org/10.1016/j.identj.2025.105180.

3. P. I. Brånemark, R. Adell, U. Breine, B. O. Hansson, J. Lindström, and A. Ohlsson, "Intra-Osseous Anchorage of Dental Prostheses. I. Experimental Studies," *Scandinavian Journal of Plastic and Reconstructive Surgery* 3, no. 2 (1969): 81–100, https://doi.org/10.3109/02844316909036699.

4. S.-S. Gao, Y.-R. Zhang, Z.-L. Zhu, and H.-Y. Yu, "Micromotions and Combined Damages at the Dental Implant/Bone Interface," *International Journal of Oral Science* 4, no. 4 (2012): 182–188, https://doi.org/10.1038/ijos.2012.68.

5. A. Hoornaert, L. Vidal, R. Besnier, J. F. Morlock, G. Louarn, and P. Layrolle, "Biocompatibility and Osseointegration of Nanostructured Titanium Dental Implants in Minipigs," *Clinical Oral Implants Research* 31, no. 6 (2020): 526–535, https://doi.org/10.1111/clr.13589.

6. G. S. Chatzopoulos and L. F. Wolff, "Dental Implant Failure and Factors Associated With Treatment Outcome: A Retrospective Study," *Journal of Stomatology, Oral and Maxillofacial Surgery* 124, no. 2 (2023): 101314, https://doi.org/10.1016/j.jormas.2022.10.013.

7. Z. R. Zhou, H. Yu, J. Zheng, L. M. Qian, Y. Yan, *Dental Biotribology*, (Springer New York, 2013) NY2013, https://doi.org/10.1007/978-1-4614-4550-0.

8. A. Hanif, S. Qureshi, Z. Sheikh, and H. Rashid, "Complications in Implant Dentistry," *European Journal of Dermatology* 11, no. 1 (2017): 135–140, https://doi.org/10.4103/ejd.ejd_340_16.

9. G. L. Kavya, A. Kumar K, G. S. Penmetsa, et al., "Enhancing Dental Implant Biocompatibility: A Systematic Review of Photo-functionalization Strategies," *Journal of Oral and Maxillofacial Surgery, Medicine, and Pathology* 38, no. 2 (2025): 189–195, https://doi.org/10.1016/j.ajoms.2025.09.017.

10. S. J. Sadowsky, "Occlusal Overload With Dental Implants: A Review," *International journal of implant dentistry* 5, no. 1 (2019): 29, https://doi.org/10.1186/s40729-019-0180-8.

11. A. Monje, A. Ravidà, H. L. Wang, J. A. Helms, and J. B. Brunski, "Relationship Between Primary/Mechanical and Secondary/Biological Implant Stability," *International Journal of Oral & Maxillofacial Implants* 34 (2019): s7–s23, https://doi.org/10.11607/jomi.19suppl.g1.

12. B. Houshmand, M. F. Ramandi, Z. Shooshtari, S. Patel, and H. Sabri, "Corticalization Around Dental Implants: A Narrative Review of the Literature," *Journal of Oral and Maxillofacial Surgery, Medicine, and Pathology* 37, no. 5 (2025): 857–863, https://doi.org/10.1016/j.ajoms.2025.05.010.

13. X. J. Gao, M. Fraulob, and G. Haïat, "Biomechanical Behaviours of the Bone–Implant Interface: A Review," *Journal of the Royal Society Interface* 16, no. 156 (2019): 20190259, https://doi.org/10.1098/rsif.2019.0259.

14. K. J. e.a.J. D. R. Chrcanovic Br, "Factors Influencing Early Dental Implant Failures," *British Dental Journal* 222, no. 4 (2017): 260, https://doi.org/10.1038/sj.bdj.2017.167.

15. E. Sánchez, E. de Vries, D. Matthews, E. van der Heide, and D. Janssen, "The Effect of Coating Characteristics on Implant-Bone Interface Mechanics," *Journal of Biomechanics* 163 (2024): 111949, https://doi.org/10.1016/j.jbiomech.2024.111949.

16. Z. R. Zhou and M. H. Zhu, *Dual-Motion Fretting Wear* (Shanghai jiaotong University Press, 2004).

17. D. Koç, A. Dogan, and B. Bek, "Effect of Gender, Facial Dimensions, Body Mass Index and Type of Functional Occlusion on Bite Force," *Journal of Applied Oral Science* 19, no. 3 (2011): 274–279, https://doi.org/10.1590/s1678-77572011000300017.

18. Q. F. Hashmi, C. Rinderknecht, C. R. Leles, and M. Srinivasan, "Reliability of a New Bite Force Device for Measuring Occlusal Bite Force in Healthy Dentate Subjects," *Journal of Dentistry* 163 (2025): 106161, https://doi.org/10.1016/j.jdent.2025.106161.

19. J. Zhang, S. Yuan, and W. J. Shen, "Three-Dimensional Finite Element Analysis of the Effects of Anatomical Occlusion and Lingualized Occlusion on Alveolar Bone and Mucosa in Mandibular Class IV edentulous jEws(in ChinJawsI)" *Journal of Hebei Medical University* 44, no. 10 (2023): 1196–1204, https://link.cnki.net/urlid/13.1209.R.20231219.1138.002.

20. J. Li, L. Hua, W. Wang, C. Gu, J. Du, and C. Hu, "Flexible, High-Strength Titanium Nanowire for Scaffold Biomimetic Periodontal Membrane," *Biosurface and Biotribology*, no. 1 (2021): 7.

21. L. Hua, C. Hu, J. Li, B. Huang, and J. Du, "Mechanical Characterization of TiO2 Nanowires Flexible Scaffold by Nano-Indentation/Scratch," *Journal of the Mechanical Behavior of Biomedical Materials* 126 (2022): 105069, https://doi.org/10.1016/j.jmbbm.2021.105069.

22. L. Hua, W. Jiang, J. Zhang, et al., "Tribo-Mechanical Responsive Ti-Based Nanowire Scaffolds Promote Osteoblast Growth," *Tribology International* 190 (2023): 109082, https://doi.org/10.1016/j.triboint.2023.109082.

23. W. Jiang, Z. Yang, H. Yan, et al., "Ti-Based Flexible Nanowire-Textured Surface Increases the Friction Coefficient Without Increasing Surface Wear," *Biosurface and Biotribology* 11, no. 1 (2025): e70013, https://doi.org/10.1049/bsb2.70013.

24. Z. Yang, W. Jiang, H. Yan, et al., "Tribological Properties of Ti-Based Nanofiber-Cs Composite Flexible Coatings," *Biosurface and Biotribology* 11, no. 1 (2025): e70001, https://doi.org/10.1049/bsb2.70001.

25. X. Wen, F. Pei, Y. Jin, and Z. Zhao, "Exploring the Mechanical and Biological Interplay in the Periodontal Ligament," *International Journal of Oral Science* 17, no. 1 (2025): 23, https://doi.org/10.1038/s41368-025-00354-y.

26. B. Wilmes and D. Drescher, "Impact of Bone Quality, Implant Type, and Implantation Site Preparation on Insertion Torques of Mini-Implants Used for Orthodontic Anchorage," *International Journal of Oral and Maxillofacial Surgery* 40, no. 7 (2011): 697–703, https://doi.org/10.1016/j.ijom.2010.08.008.

27. C.-L. Chang, J.-J. Chen, and C.-S. Chen, "Using Optimization Approach to Design Dental Implant in Three Types of Bone Quality—A Finite Element Analysis," *Journal of Dental Science* 20, no. 1 (2025): 126–136, https://doi.org/10.1016/j.jds.2024.09.017.

28. C. Lü, S. Zheng, and S. Zhang, "Three-Dimensional Finite Element Analysis of the Effect of Carbon Nanotube-Modified High-Density Polyethylene Antibacterial Buffer Layer on Stress Distribution of Implants," (In Chinese) *Zhejiang Clinical Medical Journal* 25, no. 9 (2023): 1279–1282, https://doi.wanfangdata.com.cn/10.3969/j.issn.1008-7664.2023.09.005.

29. Q. Zhong, Z. Zhai, Z. A. Wu, et al., "Thread Design Optimization of a Dental Implant Using Explicit Dynamics Finite Element Analysis," *Scientific Reports* 15, no. 1 (2025): 23868, https://doi.org/10.1038/s41598-025-08858-7.

30. F. Sun, L. Xu, J. Han, H. Xu, X. Li, and Z. Lin, "Effect of the Connection Structure of Zirconia Dental Implants on Biomechanical Properties," *Journal of the Mechanical Behavior of Biomedical Materials* 161 (2025): 106800, https://doi.org/10.1016/j.jmbbm.2024.106800.

31. M. A. Khalifah, "Impact of Chewing Side Preference on Bite Force, Muscle Activity, and the Development of Temporomandibular Joint Disorders," *Journal of Maxillofacial and Oral Surgery* (2025): 1–5, https://doi.org/10.1007/s12663-025-02711-0.

32. M. Bakke, "Bite Force and Occlusion," *Seminars in Orthodontics* 12, no. 2 (2006): 120–126, https://doi.org/10.1053/j.sodo.2006.01.005.

33. R. A. M. de Abreu, M. D. Pereira, F. Furtado, G. P. R. Prado, W. Mestriner, and L. M. Ferreira, "Masticatory Efficiency and Bite Force in Individuals With Normal Occlusion," *Archives of Oral Biology* 59, no. 10 (2014): 1065–1074, https://doi.org/10.1016/j.archoralbio.2014.05.005.

34. F. Fontijn-Tekamp, A. Slagter, A. Van Der Bilt, et al., "Biting and Chewing in Overdentures, Full Dentures, and Natural Dentitions," *Journal of Dental Research* 79, no. 7 (2000): 1519–1524, https://doi.org/10.1177/00220345000790071501.

35. J. John, V. Rangarajan, R. C. Savadi, K. S. Satheesh Kumar, and P. Satheesh Kumar, "A Finite Element Analysis of Stress Distribution in the Bone, Around the Implant Supporting a Mandibular Overdenture With Ball/o Ring and Magnetic Attachment," *Journal of Indian Prosthodontic Society* 12, no. 1 (2012): 37–44, https://doi.org/10.1007/s13191-012-0114-0.